SCIENTIFIC REPORTS

OPEN

SUBJECT AREAS:
MATERIALS PHYSICS
ELECTRONIC MATERIALS AND DEVICES
MATERIALS CHEMISTRY
MAGNETIC MATERIALS AND DEVICES

Received
1 May 2012

Accepted
25 May 2012

Published
11 June 2012

Correspondence and requests for materials should be addressed to Y.S. (shimak@scl.kyoto-u.ac.jp)

Ligand-hole localization in oxides with unusual valence Fe

Wei-Tin Chen[1], Takashi Saito[1], Naoaki Hayashi[2], Mikio Takano[3] & Yuichi Shimakawa[1,4]

[1]Institute for Chemical Research, Kyoto University, Uji, Kyoto 611-0011, Japan, [2]Micro/Nano Fabrication Hub, Center for the Promotion of Interdisciplinary Education and Research, Kyoto University, Kyoto 606-8501, Japan, [3]Institute for Integrated Cell-Material Sciences, Kyoto University, Kyoto 606-8501, Japan, [4]Japan Science and Technology Agency, CREST, Uji, Kyoto 611-0011, Japan.

Unusual high-valence states of iron are stabilized in a few oxides. *A*-site-ordered perovskite-structure oxides contain such iron cations and exhibit distinct electronic behaviors at low temperatures, *e.g.* charge disproportionation ($4Fe^{4+} \rightarrow 2Fe^{3+} + 2Fe^{5+}$) in $CaCu_3Fe_4O_{12}$ and intersite charge transfer ($3Cu^{2+} + 4Fe^{3.75+} \rightarrow 3Cu^{3+} + 4Fe^{3+}$) in $LaCu_3Fe_4O_{12}$. Here we report the synthesis of solid solutions of $CaCu_3Fe_4O_{12}$ and $LaCu_3Fe_4O_{12}$ and explain how the instabilities of their unusual valence states of iron are relieved. Although these behaviors look completely different from each other in simple ionic models, they can both be explained by the localization of ligand holes, which are produced by the strong hybridization of iron *d* and oxygen *p* orbitals in oxides. The localization behavior in the charge disproportionation of $CaCu_3Fe_4O_{12}$ is regarded as charge ordering of the ligand holes, and that in the intersite charge transfer of $LaCu_3Fe_4O_{12}$ is regarded as a Mott transition of the ligand holes.

Iron ions in oxides usually show the +2 and +3 oxidation states typically seen in wüstite ($Fe^{2+}O$)[1,2], magnetite ($Fe^{2+}Fe^{3+}{}_2O_4$)[3–5], and hematite ($Fe^{3+}{}_2O_3$)[6,7]. A few oxides, such as $SrFeO_3$ and $CaFeO_3$, contain unusual high-oxidation-state iron ions like Fe^{4+}, and the behaviors of such high-valence iron ions have been attracting much attention for a long time[8–12]. The cubic perovskite $SrFeO_3$ shows a metallic conductivity down to low temperatures because the linear Fe^{4+}-O-Fe^{4+} bonds stabilize broad conduction bands. $CaFeO_3$, on the other hand, has a distorted perovskite structure with a Fe-O-Fe bond angle of ≈160°[13,14]. The unusual oxidation state of the Fe^{4+} in $CaFeO_3$ cannot be maintained at low temperatures, and at 290 K its instability is relieved by charge disproportionation (CD): $2Fe^{4+} \rightarrow Fe^{3+} + Fe^{5+}$ [11,12]. Charge disproportionation is also seen in some perovskite-related-structure compounds like $Sr_3Fe_2O_7$ and $La_{1-x}Ba_xFeO_{3-y}$, relieving the instability of their unusual valence states of iron[15–18].

More than five decades after $SrFeO_3$ was discovered, a new Fe^{4+}-containing material was found, which has the *A*-site-ordered double-perovskite structure (see the crystal structure in Fig. 1). $CaCu_3Fe_4O_{12}$ is obtained by synthesis under high-pressure and high-temperature conditions, and the high-valence Fe^{4+} is stabilized at room temperature[19]. At 210 K the compound shows *B*-site charge disproportionation ($4Fe^{4+} \rightarrow 2Fe^{3+} + 2Fe^{5+}$) similar to the charge disproportionation in the simple perovskite $CaFeO_3$, and it changes from a high-temperature paramagnetic-and-metallic phase to a low-temperature ferromagnetic-and-insulating phase (a charge-disproportionated phase). High-pressure synthesis techniques can be used to produce the analogous compound $LaCu_3Fe_4O_{12}$, in which La^{3+} instead of Ca^{2+} occupies the *A* site in the *A*-site-ordered perovskite structure[20]. At 393 K $LaCu_3Fe_4O_{12}$ shows not the CD behavior seen in $CaCu_3Fe_4O_{12}$ but instead exhibits *A'*-*B* intersite charge transfer (CT), $3Cu^{2+} + 4Fe^{3.75+} \rightarrow 3Cu^{3+} + 4Fe^{3+}$, and changes from a high-temperature paramagnetic-and-metallic phase to a low-temperature antiferromagnetic-and-insulating phase (a charge-transferred phase). Thus the instabilities of the unusual oxidation states of iron in these two *A*-site-ordered perovskites, Fe^{4+} in $CaCu_3Fe_4O_{12}$ and $Fe^{3.75+}$ in $LaCu_3Fe_4O_{12}$, are relieved by completely different ways. To find out how the instabilities of the unusual oxidation states of the transition-metal ions in oxides are relieved, we made solid solution of $CaCu_3Fe_4O_{12}$ and $LaCu_3Fe_4O_{12}$ and investigated their temperature-dependent transitions.

Results

Each solid-solution sample was confirmed by synchrotron X-ray diffraction (XRD) data (see Supplementary Fig. S1) to be a single phase at high temperatures and to be crystallized with a cubic *Im*-3 *A*-site-ordered double-perovskite structure. Oxygen off-stoichiometry was not detected in the Rietveld structure refinements, and the refined occupancies for Ca and La at the *A* site were within 2% of those corresponding to the designed

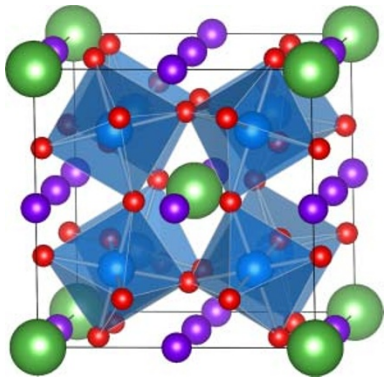

Figure 1 | Crystal structure of the *A*-site-ordered double-perovskite $AA'_3B_4O_{12}$. The *A*, *A*', *B*, and O atoms are respectively represented by green, purple, blue, and red spheres. The atom positions in the cubic *Im*-3 (No. 204) symmetry are *A* at the 2*a* site (0, 0, 0), *A*' at the 6*b* site (0, 1/2, 1/2), *B* at the 8*c* site (1/4, 1/4, 1/4), and at O at the 24*g* site (*x*, *y*, 0), where $x \approx 0.30$ and $y \approx 0.17$.

composition $Ca_{1-x}La_xCu_3Fe_4O_{12}$ (see Supplementary Fig. S1 and Supplementary Table S1 for the refinement results). When changing the *A*-site composition *x* the lattice constant at 450 K changes linearly in accordance with Vegard's law (Fig. 2a). No superlattice reflection was observed in the diffraction patterns, suggesting the absence of any extra ordering in the solid solution. Each Mössbauer spectrum at high temperatures showed a paramagnetic singlet component (Fig. 3), further confirming that each of the samples consisted of a single-phase solid solution. Note that the isomer shift values of the Mössbauer spectra of the paramagnetic states at 400 K gradually increase with increasing *x* (see Supplementary Fig. S2), suggesting that the Fe oxidation state decreases slightly. Furthermore, the bond valence sums (BVS) of Fe at 450 K, which are obtained from the structure refinements, gradually decrease with increasing *x* while those of Cu remain unchanged (Fig. 2b). The results suggest that electrons are doped into the Fe site instead of the Cu site by the La^{3+} substitution for Ca^{2+} at the *A* site. Thus, as we expected from the end compositions, the ionic formula of a solid-solution sample at high temperature can be described as $(Ca^{2+}{}_{1-x}La^{3+}{}_x)Cu^{2+}{}_3Fe^{(4-x/4)+}{}_4O_{12}$.

For $CaCu_3Fe_4O_{12}$ ($x = 0.0$) a phase transition at 210 K is evident in the temperature dependence of the lattice parameter (Fig. 2c), and below that temperature very weak superstructure peaks, indicating rock-salt-type *B*-site ordering, were observed in the synchrotron XRD patterns. The ferrimagnetic transition (Fig. 4) and the metal-to-insulator transition (see Supplementary Fig. S3), together with the change in the Mössbauer spectra (Fig. 3a), confirm that the *B*-site CD occurs at 210 K, as we reported previously[19,21]. In the other end compound $LaCu_3Fe_4O_{12}$ ($x = 1.0$), a first-order isostructural phase transition takes place at 393 K, as shown by the large increase of the lattice parameter with decreasing temperature (Fig. 2c). At the transition temperature the Fe-O bond length increases significantly whereas the Cu-O bond length decreases, decreasing the BVS for Fe and increasing it for Cu. From the Mössbauer spectra shown in Fig. 3b, one can infer that above the transition temperature there is a paramagnetic component of unusual high-valence Fe that has an isomer shift of $\approx$0.17 mm s^{-1} and that at 300 K there is a single component of magnetically ordered Fe^{3+}. In addition, the compound changes from a high-temperature paramagnetic metal to a low-temperature antiferromagnetic insulator at the phase transition (Fig. 4 and Supplementary Fig. S3). Thus it is concluded that the compound changes from a high-temperature $La^{3+}Cu^{2+}{}_3Fe^{3.75+}{}_4O_{12}$ phase to a low-temperature $La^{3+}Cu^{3+}{}_3Fe^{3+}{}_4O_{12}$ phase as a result of the intersite CT between the *A*'-site Cu and *B*-site Fe. No CD behavior, either that shown by $CaCu_3Fe_4O_{12}$ or the more complicated one shown by $La_{1-x}Sr_xFeO_{3-\delta}$[22–24], is seen in $LaCu_3Fe_4O_{12}$[20,25].

The temperature dependence of the XRD patterns of the $Ca_{3/4}La_{1/4}Cu_3Fe_4O_{12}$ sample ($x = 1/4$) shows electronic phase separation below 210 K (Supplementary Fig. S4). The large increase in the lattice parameter at 210 K with decreasing temperature indicates the appearance of the CT phase (Fig. 2c). On the other hand, the temperature dependence of the magnetic susceptibility shows a behavior similar to that shown by $CaCu_3Fe_4O_{12}$, namely a sharp ferrimagnetic increase below $\approx$210 K but with a lower magnetization (Fig. 4) indicative of the CD transition. These are consistent with the Mössbauer spectrum at 4 K shown in Fig. 3c, which consists of a pair of Fe^{3+}/Fe^{5+} (29.6%/28.5%) components for the

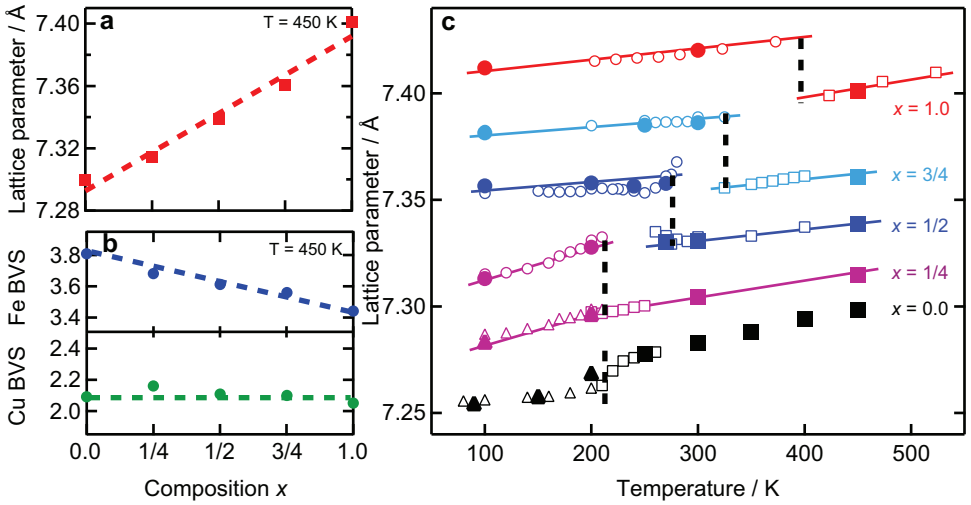

Figure 2 | Composition and temperature dependences of the lattice parameter of the $Ca_{1-x}La_xCu_3Fe_4O_{12}$ solid solution. (a) Lattice parameters of the high-temperature phases at 450 K plotted as a function of composition *x*. The linear change follows Vegard's law, confirming that the samples are solid solutions. (b) BVS changes for Fe (blue) at the *B* site and Cu (green) at the *A*' site in the high-temperature phase of the $Ca_{1-x}La_xCu_3Fe_4O_{12}$ solid solution. BVS was calculated from the results of the structure refinements for the synchrotron XRD data obtained at 450 K. (c) Temperature dependence of lattice parameters of solid-solution samples. Data shown by closed symbols were obtained from synchrotron XRD and data shown by open symbols were obtained from laboratory XRD with Mo and Cu sources. The square, circle and triangle markers represent the high-temperature, charge-transferred and charge-disproportionated phases, respectively. Negative ($\Delta a < 0$ with increasing *T*) and positive ($\Delta a > 0$ with increasing *T*) thermal-expansion-like changes respectively indicate intersite CT and the CD transitions.

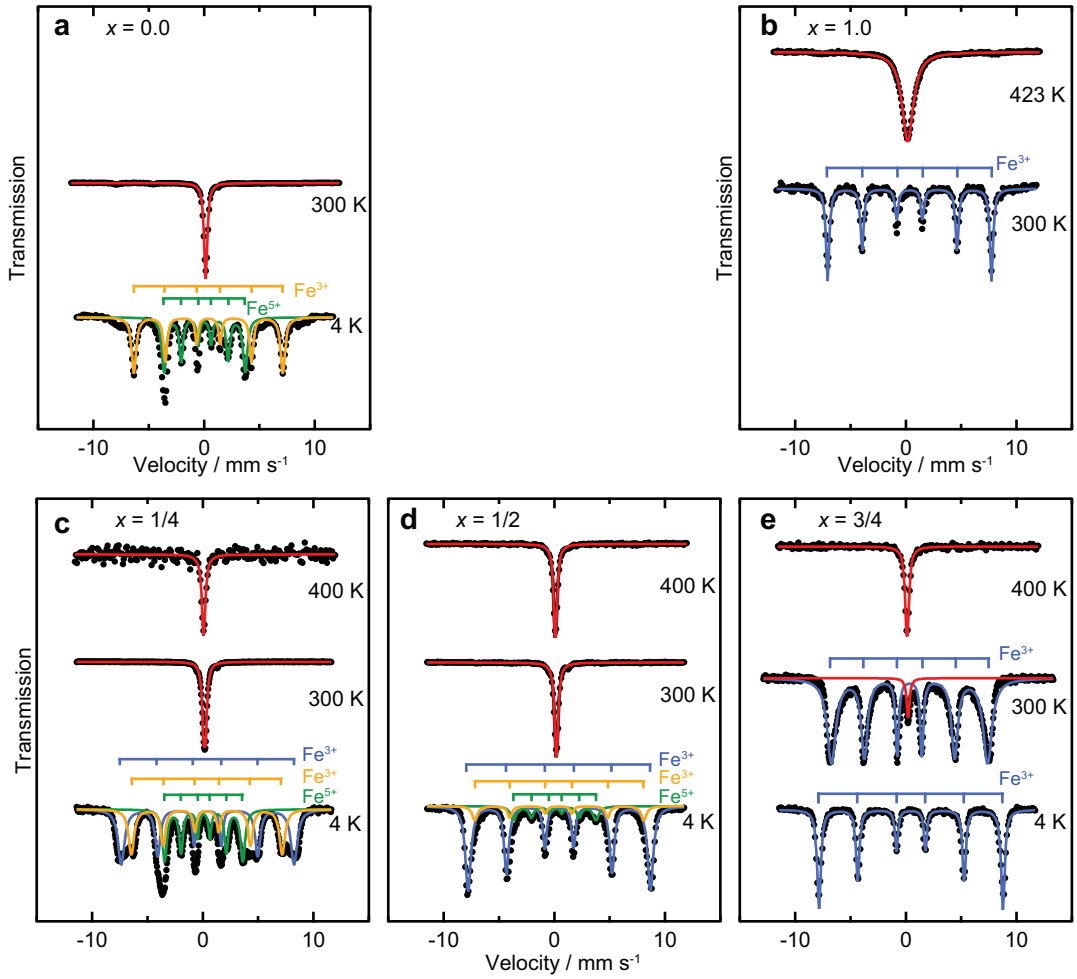

Figure 3 | Mössbauer spectra of the $Ca_{1-x}La_xCu_3Fe_4O_{12}$ solid solution at selected temperatures. The observed spectra and fitting curves are represented by dots and solid lines, respectively. The high-temperature spectra shown in red have a single component due to paramagnetic high-valence Fe, and each the low-temperature spectrum shown in blue is a magnetically ordered Fe^{3+} sextet originating from the phase due to CT. The spectra shown in orange and green are respectively those of charge-disproportionated Fe^{3+} and Fe^{5+}. Note that the spectrum weights of Fe^{3+} and Fe^{5+} in the charge-disproportionated phase are always close to 1 : 1.

charge-disproportionated phase and a magnetic ordered Fe^{3+} component (41.9%) for the phase due to CT. It is thus clear that below 210 K phases due to CD and CT coexist.

When the further La-doped $Ca_{1/2}La_{1/2}Cu_3Fe_4O_{12}$ ($x = 1/2$) is cooled its lattice parameter increases sharply at 280 K (Fig. 2c), suggesting the occurrence of CT. Note that at low temperatures its diffraction peaks are rather broad (Supplementary Fig. S4). In the magnetic susceptibility data, a sharp decrease is found at 280 K, also indicating a CT transition like that in $LaCu_3Fe_4O_{12}$. When the sample was further cooled, a CD-like increase was seen near 210 K, although the magnetization is more than an order of magnitude lower than that of $CaCu_3Fe_4O_{12}$ at low temperatures (Fig. 4). The Mössbauer spectra change accordingly with decreasing temperature (Fig. 3d). A single paramagnetic component is seen at high temperatures, and in the spectrum at 228 K a sextet (82%) originating from magnetically ordered Fe^{3+} is seen in addition to the high-temperature singlet (18%). At 4 K the high-temperature singlet changes to a Fe^{3+}/Fe^{5+} sextet pair (refined area of each component: 12.8%/11.9%), confirming that CD occurs in roughly 25% of the sample.

For $Ca_{1/4}La_{3/4}Cu_3Fe_4O_{12}$ ($x = 3/4$) the changes in the temperature-dependence of the XRD patterns (Supplementary Fig. S4) and the lattice parameters derived from them (Fig. 2c) indicate that intersite CT transition occurs around 330 K. In the Mössbauer spectra a paramagnetic component of high-valence Fe with an isomer shift 0.12 mm s^{-1} is seen at 400 K, while a single component from magnetically ordered Fe^{3+} is seen at 4 K, suggesting that most of the sample undergoes a CT transition (Fig. 3e). These CT behaviors are consistent with the observed sharp decrease in the magnetic susceptibility (Fig. 4) and the large increase in the resistivity below 330 K (Supplementary Fig. S3). Although a very minor CD-like transition around 210 K is seen in the magnetic susceptibility measurement, the charge-disproportionated phase is not as evident in the Mössbauer spectra and the XRD patterns.

A compositional phase diagram of the $Ca_{1-x}La_xCu_3Fe_4O_{12}$ solid solution is derived from all the experimental results described above and is shown in Fig. 5. For $CaCu_3Fe_4O_{12}$ ($x = 0.0$) a CD transition is seen at 210 K. For $x = 1/4$ both CD and CT transitions are seen at almost the same temperature, ≈210 K, where about 60% of the sample shows CD while the other 40% shows CT. For $x = 1/2$, around 280 K CT occurs on cooling in about 75% of the sample and the other 25% remains in the high-temperature state with unusually high-valence Fe. The remaining high-temperature phase then undergoes CD at 210 K, which is the same as the CD transition temperature for the $x = 0.0$ sample. Below this temperature, phases due to CD and CT coexist. For $x = 3/4$ the CT transition occurs around 330 K in most of the sample and a very minor charge-disproportionated phase appears below 210 K. And for $LaCu_3Fe_4O_{12}$ ($x = 1.0$), only CT transition is observed at 393 K. In summary, the intersite CT transition temperatures (T_{CT})

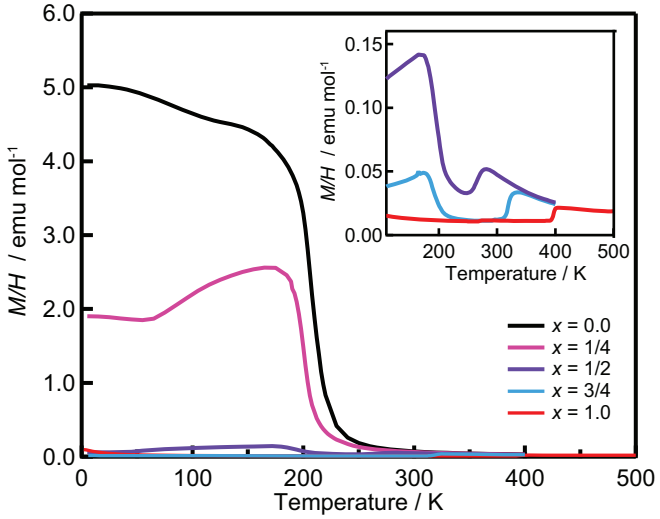

Figure 4 | Temperature dependence of the magnetic susceptibility of the $Ca_{1-x}La_xCu_3Fe_4O_{12}$ solid solution. The samples were zero-field cooled and the measurements were made under a 1 T external magnetic field. The large increase in magnetization at 210 K indicates the ferrimagnetic transition accompanying the CD transition. The inset shows the magnified view of temperature dependence of the magnetic susceptibility of samples with $x = 1/2$, 3/4 and 1.0. The decrease in magnetic susceptibility is the result of antiferromagnetism due to the intersite CT transition.

in the solid solution samples increase with increasing La doping (*i.e.*, with increasing x), while the CD transition temperatures (T_{CD}) do not change from that of $CaCu_3Fe_4O_{12}$.

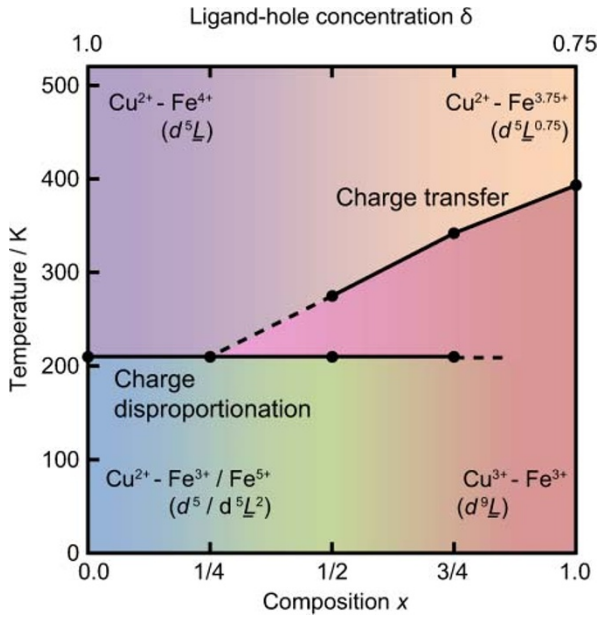

Figure 5 | Compositional phase diagram for the $Ca_{1-x}La_xCu_3Fe_4O_{12}$ solid solution. At high temperatures the whole solid solution is a single phase. Different charge behaviors are seen in the end-composition compounds: CD in $CaCu_3Fe_4O_{12}$ ($x = 0.0$) and intersite CT in $LaCu_3Fe_4O_{12}$ ($x = 1.0$). In the intermediate-composition samples, phases due to both CD and CT coexist at low temperatures. With increasing ligand-hole concentration δ (decreasing La substitution at the A site), T_{CT} decreases but T_{CD} remains constant.

Discussion

Note again that at high temperatures each solid-solution sample is a single phase and that the A-site substitution of La^{3+} for Ca^{2+} causes electron doping at the B-site Fe. Nevertheless, the electronic phase separation in the samples with the intermediate compositions is clearly seen at low temperatures. For $x = 1/2$, for example, the high-temperature phase can be described as $ACu^{2+}{}_3Fe^{3.875+}{}_4O_{12}$, and the CT transition at 330 K changes some portion of the sample to $ACu^{3+}{}_3Fe^{3+}{}_4O_{12}$, leaving the remaining portion of the sample to be a phase with unusually high-valence Fe. In a simple ionic model, this change can be described as $ACu^{2+}{}_3Fe^{3.875+}{}_4O_{12} \rightarrow 50\%ACu^{3+}{}_3Fe^{3+}{}_4O_{12} + 50\%ACu^{2+}{}_3Fe^{4+}{}_4O_{12}$. Although such an electronic phase-separation behavior seems to be uncommon, we could never observe a transition of the whole sample, such as a CT-like $ACu^{2+}{}_3Fe^{3.875+}{}_4O_{12} \rightarrow ACu^{3+}{}_3Fe^{3.125+}{}_4O_{12}$ transition or a CD-like $ACu^{2+}{}_3Fe^{3.875+}{}_4O_{12} \rightarrow ACu^{2+}{}_3Fe^{3+}{}_{2.25}Fe^{5+}{}_{1.75}O_{12}$ transition. Further decreasing temperature induces the CD transition for the $ACu^{2+}{}_3Fe^{4+}{}_4O_{12}$ portion at 210 K, where $ACu^{2+}{}_3Fe^{3+}{}_2Fe^{5+}{}_2O_{12}$ is stabilized. Although the observed fractions of the CT and CD phases (75%/25%) determined from the areas of the Mössbauer spectra measured at 4 K are rather different from the 50%/50% fractions predicted by the simple ionic model, they are reasonably close to the predicted ones. An important point is that the Fe^{3+}:Fe^{5+} ratios in the CD phases are always close to 1 : 1. Furthermore, none of the T_{CD} of the samples changes with composition x, suggesting that the observed CD transitions are essentially the same in the entire solid solution. The XRD peak broadening seen at low temperatures strongly suggests that the domains of the phases due to CD and CT coexist on a microscopic scale.

Why are the instabilities of these unusual oxidation states of Fe relieved in different ways? And why do we see both the CD and CT transitions in a single-phase sample? As discussed in previous reports on some specific oxides, high-oxidation-state transition-metal ions like Fe, Co, Ni, and Cu have very low-lying 3*d* levels, and the covalent electronic states due to the strong hybridization of 3*d* and oxygen 2*p* orbitals produce oxygen p holes (ligand holes)[26–35]. Thus, realistic electronic pictures of the unusual Fe^{4+}, Fe^{5+}, and Cu^{3+} states can respectively be described as $d^5\underline{L}$, $d^5\underline{L}^2$, and $d^9\underline{L}$, where $\underline{L}$ represent a ligand hole. Indeed, unlike the isoelectric Mn^{3+} ($t_{2g}{}^3e_g{}^1$), Fe^{4+} (d^4) with octahedral oxygen coordination does not show Jahn-Teller distortion. With the ligand-hole picture, CD in $CaCu_3Fe_4O_{12}$ is expressed as ($4d^5\underline{L} \rightarrow 2d^5 + 2d^5\underline{L}^2$), similar to that in $CaFeO_3$. The transition is regarded as a redistribution of the ligand holes in the Fe sites, making the Fe-O bonds alternately shorter and longer in a rock-salt-type manner (Fig. 6a). The rock-salt-type ordering should contribute to minimizing the lattice energy and stabilizing the CD phase. Because at high temperatures the ligand holes are itinerant, as we see in the metallic conductivity, the CD transition in $CaCu_3Fe_4O_{12}$ can be regarded as the localization of the ligand holes at the Fe sites, or in other words, as a charge ordering of the ligand holes. In $LaCu_3Fe_4O_{12}$, on the other hand, the CT between the A'-site Cu ions and the B-site Fe ions is mediated by the transfer of ligand holes ($3d^9 + 4d^5\underline{L}^{0.75} \rightarrow 3d^9\underline{L} + 4d^5$) from the Fe site to the Cu site (Fig. 6c). This ligand-hole transfer is also linked to the lattice change with the isotropic volume expansion. Since the charge transferred phase is insulating, the intersite CT transition can also be regarded as the localization of the ligand holes at the Cu site. Since the observed metal-to-insulator transition is caused by the localization of an odd number of itinerant ligand holes without breaking the cubic structural symmetry, it can be regarded as a Mott transition of the igand holes. It is clear that the difference between the CD and CT transitions is only the localization site of the ligand holes, so the energy difference between them should not be significant. This also explains why the charge-disproportionated and the charge-transferred phases coexist in the solid solution.

At high temperatures the ligand holes in the solid solution are homogeneously distributed at the Fe sites like $d^5\underline{L}^{\delta}$ ($\delta = 1-x/4$)

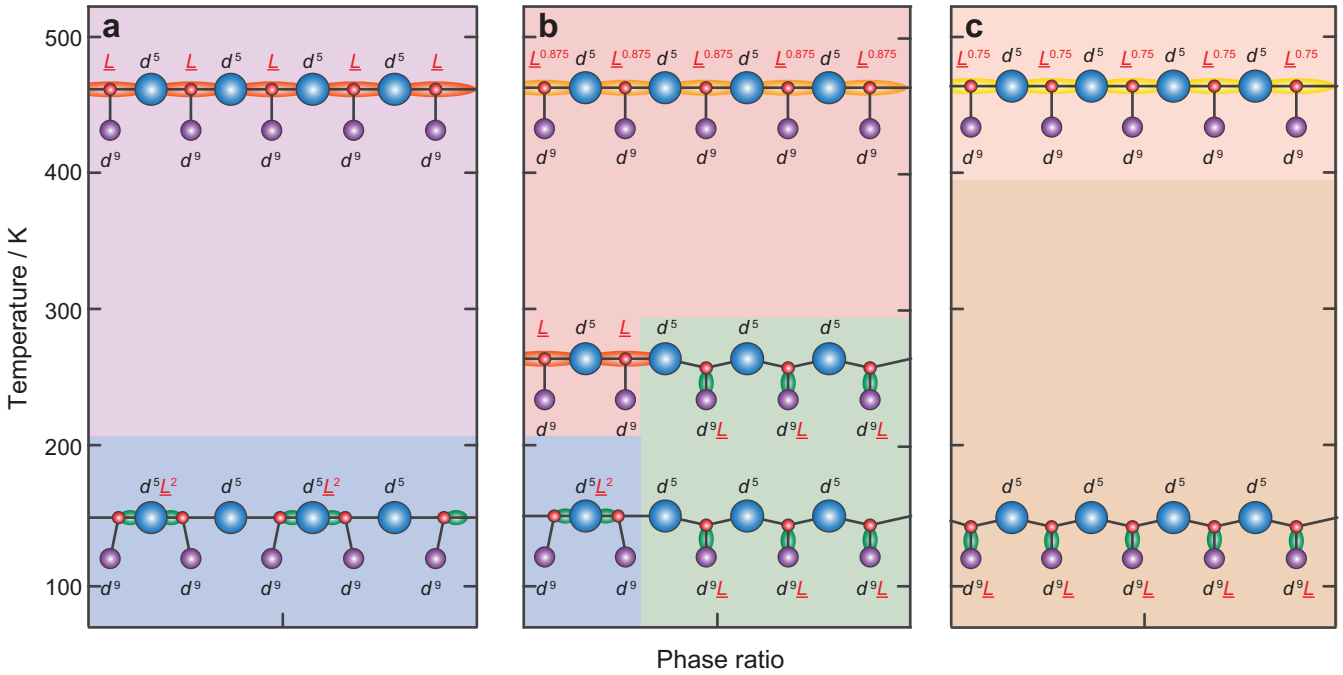

Figure 6 | Ligand-hole localization model of charge disproportionation and intersite charge-transfer transition behaviors. At high temperatures the ligand holes $\underline{L}$ are homogeneously distributed at the Fe sites, and here the ligand-hole concentration increases from (c) to (a). (a) The CD ($4Fe^{4+} \rightarrow 2Fe^{3+} + 2Fe^{5+}$) at 210 K in $CaCu_3Fe_4O_{12}$ is described as $4d^5\underline{L} \rightarrow 2d^5 + 2d^5\underline{L}^2$ and can be regarded as the localization of the ligand holes at the Fe site (charge ordering of $\underline{L}$). (c) The intersite CT ($3Cu^{2+} + 4Fe^{3.75+} \rightarrow 3Cu^{3+} + 4Fe^{3+}$) at 393 K in $LaCu_3Fe_4O_{12}$ is described as $3d^9 + 4d^5\underline{L}^{0.75} \rightarrow 3d^9\underline{L} + 4d^5$ and can be regarded as the localization of the ligand holes at the Cu site (a Mott transition of $\underline{L}$). (b) In the intermediate-composition samples (*e.g.*, $x = 1/2$), with decreasing temperature the ligand holes are first localized at the Cu site by making CT-phase domains (about 75% of the sample). When temperature decreases further, the ligand holes in the other portion (25%) of the sample are localized at the Fe site, making CD-phase domains.

and they are itinerant. When temperature decreases, the ligand holes lose kinetic energy and become unstable, resulting in the localization. The instability of the itinerant ligand holes is first relieved by transferring the ligand holes from the Fe site to the Cu site, and the localization at the Cu site produces the $d^9\underline{L}$ state. This also explains the change of the T_{CT} in the solid solution. Because the ligand-hole concentration δ increases with decreasing x, the high-temperature state with a higher concentration of the itinerant holes is more stable over a wider temperature range and thus the T_{CT} decreases. The Cu^{2+} counter cation in the *A*-site-ordered perovskite-structure oxide plays a crucial role in accepting the ligand holes. It is also interesting that the CT transition in the intermediate compositions does not occur in the whole sample but leaves some portion (domains) with itinerant ligand holes at the Fe site, causing an electronic phase separation. With further decreasing temperature, the instability of the remaining itinerant ligand holes is relieved by CD in which the $d^5/d^5\underline{L}^2$ states are ordered alternately (Fig. 6b). In the higher ligand-hole-concentration region ($0.0 \leq x \leq 1/4$), T_{CT} is lower than (or almost the same as) T_{CD}, and thus the CT is not observed.

In conclusion, the unusual high-valence Fe ions are stabilized in the high-pressure synthesized *A*-site-ordered perovskite-structure $Ca_{1-x}La_xCu_3Fe_4O_{12}$ solid-solution samples, and the end-composition compounds $CaCu_3Fe_4O_{12}$ and $LaCu_3Fe_4O_{12}$ display distinct charge behaviors, respectively charge disproportionation (CD) and intersite charge transfer (CT). Compounds with intermediate compositions first show intersite CT transition in part of the sample and then show CD in the rest of the sample. In this system, *d* orbitals of Fe at the *B* site and Cu at the *A'* site strongly hybridize with *p* orbitals of oxygen, producing ligand holes, and the distinct charge behaviors can be explained by the localization of the itinerant ligand holes at low temperatures. In the charge-disproportionated phase the ligand holes are localized at the Fe site and the transition is regarded as one to the rock-salt-type charge ordering of the ligand holes. The CD transition is essentially the same in all solid-solution samples, so the T_{CD} is same regardless of their La content. In the intersite CT, on the other hand, the ligand holes are localized at the Cu site and the transition can be regarded as a Mott transition of the ligand holes. T_{CT} decreases with increasing concentration of the ligand-hole carriers. In the *A*-site-ordered perovskite-structure oxides, transition-metals at both *A'* and *B* sites mediate *A'*-*A'*, *A'*-*B*, and *B*-*B* interactions that lead to intriguing physical properties[36–41]. The ligand holes produced by the strong hybridization of transition-metal cation *d* orbitals and oxygen *p* orbitals also play important roles in giving rise to various electronic and structural properties. The present *A*-site-ordered perovskite-structure $Ca_{1-x}La_xCu_3Fe_4O_{12}$ solid solution is a novel example exhibiting interplay of the interactions mediated by the ligand holes.

Methods

Polycrystalline samples of the *A*-site-ordered double-perovskite solid solution $Ca_{1-x}La_xCu_3Fe_4O_{12}$ (x = 0.0, 1/4, 1/2, 3/4 and 1.0) were prepared, at 15 GPa and 1300 K, from stoichiometric amounts of $Ca_2Fe_2O_5$, La_2O_3, CuO, Fe_2O_3, and the oxidizing agent $KClO_4$ by using a multianvil press. Synchrotron XRD patterns at temperatures between 100 and 450 K were collected at beamline BL02B2, SPring-8, Japan, with wavelength 0.7737405 Å, and the profiles were analyzed with Rietveld method by using the General Structure Analysis System (GSAS) software package[42,43]. The XRD patterns at temperatures between 80 and 400 K were also collected using a Rigaku RINT diffractometer with a Mo and a Cu source. Magnetic susceptibility, magnetization, and electric conductivity were measured using a Quantum Design Magnetic Properties Measurement System (MPMS) and Quantum Design Physical Properties Measurement System (PPMS). The ^{57}Fe Mössbauer spectra were obtained in transmission geometry in combination with a constant-acceleration spectrometer using ^{57}Co/Rh as a radiation source. α-Fe was used as a control for velocity calibration and isomer shift. The obtained spectra were fitted by a least-squares method with Lorentzian functions.

1. Jette, E. R. & Foote, F. An X-ray study of the wüstite (FeO) solid solutions. *J. Chem. Phys.* **1**, 29–36 (1933).

2. Hazen, R. M. & Jeanloz, R. Wüstite ($Fe_{1-x}O$): A review of its defect structure and physical properties. *Rev. Geophys.* **22**, 37–46 (1984).
3. Bragg, W. H. The structure of magnetite and the spinels. *Nature* **95**, 561 (1915).
4. Verwey, E. J. W. Electronic conduction of magnetite (Fe_3O_4) and its transition point at low temperatures. *Nature* **144**, 327–328 (1939).
5. Senn, M. S., Wright, J. P. & Attfield, J. P. Charge order and three-site distortions in the Verwey structure of magnetite. *Nature* **481**, 173–176 (2012).
6. Pauling, L. & Hendricks, S. B. The crystal structures of hematite and corundum. *J. Am. Chem. Soc.* **47**, 781–790 (1925).
7. Hoefer, H. E., Brey, G. P., Schulz-Dobrick, B. & Oberhaensli, R. The determination of the oxidation state of iron by the electron microprobe. *Eur. J. Mineral.* **6**, 407–418 (1994).
8. Watanabe, H. Magnetic properties of perovskites containing strontium I. Strontium-rich ferrites and cobaltites. *J. Phys. Soc. Jpn.* **12**, 515 (1957).
9. Clevenger, T. R. Effect of Fe^{4+} in the system $SrFeO_3$-$SrTiO_3$. *J. Am. Ceram. Soc.* **46**, 207–210 (1963).
10. MacChesney, J. B., Sherwood, R. C. & Potter, J. F. Electric and magnetic properties of the strontium ferrates. *J. Chem. Phys.* **43**, 1907–1913 (1965).
11. Takano, M., Nakanishi, N., Takeda, Y., Naka, S. & Takada, T. Charge disproportionation in $CaFeO_3$ studied with the Mössbauer effect. *Mater. Res. Bull.* **12**, 923–928 (1977).
12. Takeda, Y. *et al.* Preparation and characterization of stoichiometric $CaFeO_3$. *Mater. Res. Bull.* **13**, 61–66 (1978).
13. Takeda, T. *et al.* Metal-semiconductor transition, charge disproportionation, and low-temperature structure of $Ca_{1-x}Sr_xFeO_3$ synthesized under high-oxygen pressure. *Solid State Sci.* **2**, 673–687 (2000).
14. Woodward, P. M., Cox, D. E., Moshopoulou, E., Sleight, A. W. & Morimoto, S. Structural studies of charge disproportionation and magnetic order in $CaFeO_3$. *Phys. Rev. B* **62**, 844 (2000).
15. Mori, K. *et al.* Crystal structure of $Sr_3Fe_2O_{7-\delta}$. *J. Phys. Chem. Solids* **60**, 1443–1446 (1999).
16. Kuzushita, K., Morimoto, S., Nasu, S. & Nakamura, S. Charge disproportionation and antiferromagnetic order of $Sr_3Fe_2O_7$. *J. Phys. Soc. Jpn.* **69**, 2767 (2000).
17. Gibb, T. C. & Matsuo, M. A study of the oxygen-deficient perovskite $Ba_{1-x}La_xFeO_{3-y}$ by Mössbauer spectroscopy. *J. Solid State Chem.* **81**, 83–95 (1989).
18. Zhang, S., Tan, S., Pi, L. & Zhang, Y. Strong correlation effects and new phase transition at high pressure-low temperature in $La_{0.5}Ba_{0.5}FeO_3$. *J. Magn. Magn. Mater.* **322**, 3381–3384 (2010).
19. Yamada, I. *et al.* A perovskite containing quadrivalent iron as a charge-disproportionated ferrimagnet. *Angew. Chem. Int. Ed.* **47**, 7032–7035 (2008).
20. Long, Y. W. *et al.* Temperature-induced A-B intersite charge transfer in an A-site-ordered $LaCu_3Fe_4O_{12}$ perovskite. *Nature* **458**, 60–63 (2009).
21. Mizumaki, M. *et al.* Direct observation of the ferrimagnetic coupling of A-site Cu and B-site Fe spins in charge-disproportionated $CaCu_3Fe_4O_{12}$. *Phys. Rev. B* **84**, 094418 (2011).
22. Takano, M., Kawachi, J., Nakanishi, N. & Takeda, Y. Valence state of the Fe ions in $Sr_{1-y}La_yFeO_3$. *J. Solid State Chem.* **39**, 75–84 (1981).
23. Battle, P. D., Gibb, T. C. & Lightfoot, P. The structural consequences of charge disproportionation in mixed-valence iron oxides. I. The crystal structure of $Sr_2LaFe_3O_{8.94}$ at room temperature and 50 K. *J. Solid State Chem.* **84**, 271–279 (1990).
24. Yang, J. B. *et al.* Charge disproportionation and ordering in $La_{1/3}Sr_{2/3}FeO_{3-\delta}$. *J. Phys: Cond. Matt.* **15**, 5093–5102 (2003).
25. Chen, W.-T., Saito, T., Attfield, J. P. & Shimakawa, Y. Charge transfer and antiferromagnetic order in the A-site-ordered perovskite $LaCu_3Fe_4O_{12}$. *J. Mater. Chem.* **20**, 7282–7286 (2010).
26. Fujimori, A., Kimizuka, N., Taniguchi, M. & Suga, S. Electronic structure of Fe_xO. *Phys. Rev. B* **36**, 6691–6694 (1987).
27. Bocquet, A. E. *et al.* Electronic structure of $SrFe^{4+}O_3$ and related Fe perovskite oxides. *Phys. Rev. B* **45**, 1561 (1992).
28. Kim, C. Y., Bedzyk, M. J., Nelson, E. J., Woicik, J. C. & Berman, L. E. Site-specific valence-band photoemission study of α-Fe_2O_3. *Phys. Rev. B* **66**, 085115 (2002).
29. van Elp, J. *et al.* Electronic structure of CoO, Li-doped CoO, and $LiCoO_2$. *Phys. Rev. B* **44**, 6090–6103 (1991).
30. Potze, R. H., Sawatzky, G. A. & Abbate, M. Possibility for an intermediate-spin ground state in the charge-transfer material $SrCoO_3$. *Phys. Rev. B* **51**, 11501–11506 (1995).
31. Fujimori, A. & Minami, F. Valence-band photoemission and optical absorption in nickel compounds. *Phys. Rev. B* **30**, 957–971 (1984).
32. van Elp, J., Eskes, H., Kuiper, P. & Sawatzky, G. A. Electronic structure of Li-doped NiO. *Phys. Rev. B* **45**, 1612 (1992).
33. Bianconi, A. *et al.* Experimental evidence of itinerant Cu($3d^9$)-oxygen-hole many body configuration in the high-*Tc* superconductor $YBa_2Cu_3O_7$. *Int. J. Mod. Phys. B* **1**, 853–862 (1987).
34. Fujimori, A., Takayama-Muromachi, E. & Uchida, Y. Electronic structure of superconducting Cu oxides. *Solid State Comm.* **63**, 857–860 (1987).
35. Bianconi, A. *et al.* Evidence of $3d^9$-ligand hole states in the superconductor $La_{1.85}Sr_{0.15}CuO_4$ from L_3 X-ray absorption spectroscopy. *Phys. Lett. A* **127**, 285–291 (1988).
36. Homes, C. C., Vogt, T., Shapiro, S. M., Wakimoto, S. & Ramirez, A. P. Optical response of high-dielectric-constant perovskite-related oxide. *Science* **293**, 673–676 (2001).
37. Kobayashi, W., Terasaki, I., Takeya, J.-i., Tsukada, I. & Ando, Y. A novel heavy-fermion state in $CaCu_3Ru_4O_{12}$. *J. Phys. Soc. Jpn.* **73**, 2373–2376 (2004).
38. Prodi, A. *et al.* Charge, orbital and spin ordering phenomena in the mixed valence manganite $(NaMn^{3+}{}_3)(Mn^{3+}{}_2Mn^{4+}{}_2)O_{12}$. *Nat. Mater.* **3**, 48–52 (2004).
39. Vasil'ev, A. N. & Volkova, O. S. New functional materials $AC_3B_4O_{12}$ (Review). *Low Temp. Phys.* **33**, 895–914 (2007).
40. Shimakawa, Y. A-site-ordered perovskites with intriguing physical properties. *Inorg. Chem.* **47**, 8562–8570 (2008).
41. Shimakawa, Y. & Saito, T. A-site magnetism in A-site-ordered perovskite-structure oxides. *Phys. Status Solidi B* **249**, 423–434 (2012).
42. Larson, A. C. & Von Dreele, R. B. General structure analysis system (GSAS). 86–748 (Los Alamos National Laboratory, 2004).
43. Toby, B. H. EXPGUI, a graphical user interface for GSAS. *J. Appl. Cryst.* **34**, 210–213 (2001).

Acknowledgments

We thank Y. W. Long and M. Azuma for help in high-pressure synthesis experiments, H. Sawa and E. Nishibori for helping in the temperature-dependent XRD measurements at Nagoya University, and J. Kim and N. Tsuji for their help with synchrotron XRD measurements at BL02B2 in SPring-8. We are also grateful to Z. Hiroi for discussion. This work was supported in part by a Grant-in-Aid for Scientific Research 19GS0207, by the Global Centers of Excellence Program "International Center for Integrated Research and Advanced Education in Materials Science," and by a grant for the Project of Integrated Research on Chemical Synthesis from the Ministry of Education, Culture, Sports, Science and Technology of Japan. The work was also supported by the Japan Science and Technology Agency's CREST program.

Author contributions

W.-T. C. and Y. S. conceived and designed the study. W.-T. C. and T. S. prepared the samples and measured the structural and physical properties. N. H. performed the Mössbauer experiments. All of the authors contributed to the interpretation and discussion of the experimental results. W.-T. C, T. S. and Y. S. wrote the manuscript.

Additional information

Supplementary information accompanies this paper at http://www.nature.com/scientificreports

Competing financial interests: The authors declare no competing financial interests.

How to cite this article: Chen, W.-T., Saito, T., Hayashi, N., Takano, M. & Shimakawa, Y. Ligand-hole localization in oxides with unusual valence Fe. *Sci. Rep.* **2**, 449; DOI:10.1038/srep00449 (2012).